Construction and Test Result of an All-REBCO Conduction-Cooled 23.5-T Magnet Prototype towards a Benchtop 1-GHz NMR Spectroscopy

Wooseung Lee, Dongkeun Park, Juan Bascuñán, and Yukikazu Iwasa

1. Francis Bitter Magnet Lab/Plasma Science and Fusion Center, Massachusetts Institute of Technology, Massachusetts.

E-mail: dk_park@mit.edu

February 2022

Abstract. A compact benchtop high-field REBCO NMR is one of the most promising HTS applications. An all-REBCO, conduction-cooled magnet is a very attractive design option for demonstrating the unique potential of REBCO for forefront magnets. In this research, we have successfully constructed and tested a prototype all-REBCO, conduction-cooled, 23.5 T magnet operating at 10 K. We have applied the concept of an extreme No-Insulation (NI) winding technique, coupled with a solder-shunting procedure to improve magnet performance. We have also used a temperature-controlled charging sequence (TCCS) to reduce the screening current. The magnet was energized to 23.6 T at 14 K; it was further operated to 25 T at 10 K for nearly 60 hours.

Keywords: All-REBCO magnet, Benchtop NMR, Cryogen-free, High-field magnet

1. Introduction

Nuclear Magnetic Resonance (NMR) spectroscopy is one of the most widely using apparatus to analyze the properties of matter: it is used in chemistry to determine molecular structures and essential in discovery and development of new drugs. In this age of shrinking resources such as space and liquid helium, and of ever-progressing probe technologies, we believe that a compact microcoil NMR spectroscopy with a 25-mm bore, i.e., a small footprint, lightweight, and less costly, is poised to take full advantage of the remarkable technological advances in conventional NMR with a standard 54-mm or larger bore [1–3]. Currently in the market, compact microcoil NMR that rely on permanent magnets are inevitably of low field (<1 T). Taking advantage of the recent progress in high-temperature superconductor (HTS), particularly for high-field (>20 T) magnet [4–8], we have proposed a benchtop cryogen-free 23.5-T/25-mm-bore magnet for 1-GHz microcoil NMR spectroscopy. We can achieve a compact design for this high-field benchtop NMR by using an all-REBCO magnet operating at($>$ 500 A/mm^2) high current density [9]. For protection of this all-REBCO 23.5-T magnet against overheating, we incorporate the no-insulation (NI) winding technique, that has become a breakthrough protection technique in HTS magnet now [10]; turn-to-turn resistance, matrix area, current density, and consequent limits of NI magnets have been explored as operating variables [11]. Because REBCO has a single thin and wide rectangular tape-like shape, its induced screening current is much greater than that of the multifilament round wire of an equivalent diameter. The screening-current-induced stress (SCS) has become one of challenging issues in high-field with HTS magnets [5]. In our previous work [9], we designed a small prototype REBCO magnet to demonstrate feasibility of the proposed benchtop 1-GHz NMR magnet. In this study, we focus on high-field performance, and all-REBCO-based magnet features. The original design has been upgraded to overcome realistic problems [12–15]. One of the upgrades is the extreme NI. Reduction of the copper matrix in the REBCO tape, of which a large portion is composed of a strong Hastelloy substrate, improves the mechanical properties of its pancake coil windings. To compensate for this matrix reduction, we added extra electrical shunting on the winding surface of each pancake with low-temperature solder ($In_{52}Sn_{48}$). We also tested a temperature-controlled charging sequence (TCCS) to minimize the SCS. This paper presents the construction and test results of a compact conduction-cooled 23.5-T all-REBCO magnet prototype operating in the temperature range of 10–50 K. Then, we present a detailed procedure for constructing the prototype magnet that includes inner joint, winding, outer joint, and assembly. Finally, we present cooling and operation steps for and results of our-proposed novel REBCO magnet that was successfully charged and operated up to 25 T.

Table 1. Magnet specifications

Parameters	C2 – C11	C1 & C12
Conductor width	6 [mm]	8 [mm]
Conductor thickness	0.057 [mm]	0.057 [mm]
Estimated minimum I_c (at 10 K)	>380 [A]	>420 [A]
I.D. (2a1)	22.23 [mm]	
O.D. (2a2)	94.6∼97.5 [mm]	
Turns per pancake	670	
Conductor total length	1.5 [km]	
Inductance (Ideal)	1.41 [H]	
I_{op}	236 [A]	
T_{op}	>10 [K]	
Peak Hoop Stress (at 50N Winding Tension, w.o. SCS)	<150 MPa	
Center Field at I_{op}	23.5 [T] – SCF (3 [T] @10 K)	

2. Magnet specification

The target center field of the prototype magnet is 23.5 T at 10 K. Table 1 shows the specifications of the magnet. The values are based on the measurement during the construction process. Some values such as O.D. of the coils became different compared to the original value [9] due to the design modification and manufacturing errors, including the non-uniform thickness of the HTS tape.

Figure 1 shows the schematic drawing of the assembled magnet. We designed the prototype magnet composed of twelve no-insulation REBCO single pancake coils and named the coils based on the assembly location; C1 is the topmost coil, and C12 is the bottommost coil. Because of the small inner winding diameter of the winding ring, we determined to use an inner joint between two single pancake coils to form a double-pancake (DP) coil topology rather than a continuous DP winding. We built a total of six DP coils with inner joints, DP coils that are connected in series with five outer joints. Kapton films are used to insulate between inner-jointed single pancake coils, and copper plates and thin-film annulus heaters are inserted between DP coils. The copper plates are used for conduction cooling, and the coil temperature is controlled by the heaters attached to the copper plates.

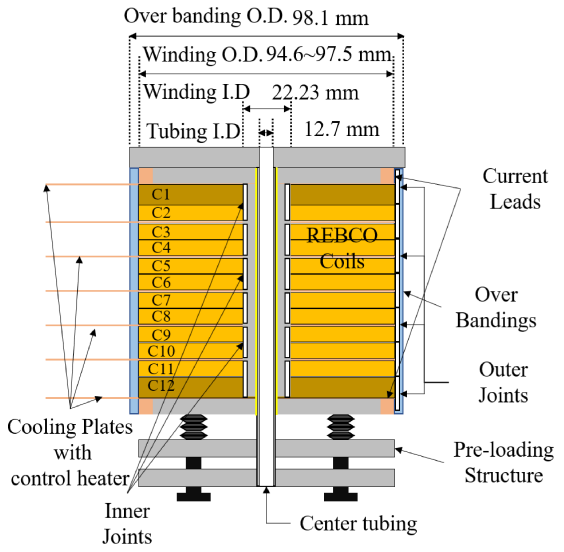

Figure 1. Schematics of the designed magnet. Pancake coils are named C1 through C12 in order from top to bottom.

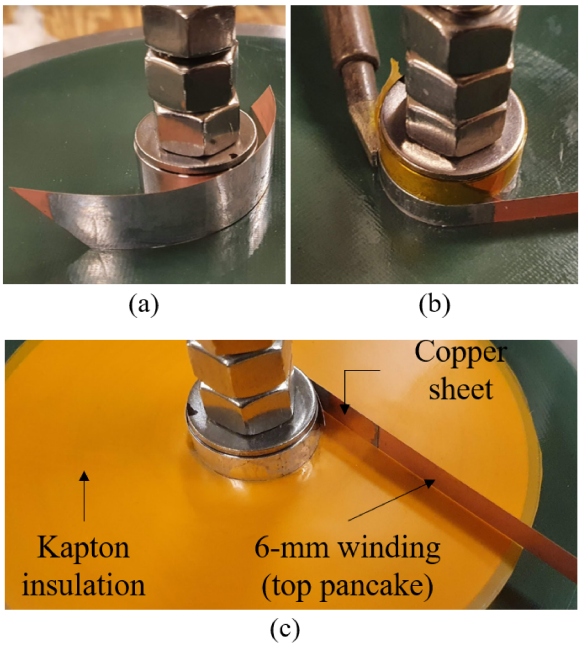

Figure 2. The inner joint. (a) is a pre-tinned 12-mm trapezoid bridge tape, (b) is the bottom joint process, (c) is the top joint process.

3. Magnet construction

3.1. Inner joint and DP winding

The DP coil winding starts from the inner joint. Figure 2 shows the 12-mm HTS REBCO tape and the bottom pancake joint process. We used this 12-mm tape to make a superconducting bridge between for the bottom and the top pancake winding. The 12-mm connects two 6-mm tapes or 6-mm tape and 8-mm tape used for the pancake winding. First, we cut the 12-mm REBCO tape into a trapezoidal shape to reduce the stress of the edge side at the starting point of winding. After the cutting, we have pre-tinned the REBCO layer side surface with eutectic $In_{52}Sn_{48}$ solder (melting point: 118 ℃), and the substrate side of the tape is affixed to the DP coil winding ring by soldering along 2–3 mm width with $Pb_{40}Sn_{60}$ solder (melting point: 190 ℃) as shown in Figure 2(a). The winding ring is made of 304 stainless still. An additional 2-mm REBCO tape was used along with the 12-mm tape for the end DP coils, C1–C2 and C11–C12, to make a flat winding surface for 8-mm width tape winding. Note that the widest available REBCO tape during this process was 12-mm. Figure 2(b) is the start of the bottom pancake winding. Once the 12-mm tape is fixed to the winding ring, we first wound the bottom pancake coil starting from the initial soldering on one end of the 12-mm tape. After we fixed the beginning point by soldering, we applied a small winding tension to the tape to press the 12-mm tape uniformly. The heat is applied to the soldered joint section by soldering iron. We also used the $In_{52}Sn_{48}$ solder, and 4-mm wide, 25-µm thick copper sheets on the pancake coil winding tape at the endpoints of the soldering section to mechanically reinforce and thus to prevent delamination of the coil winding tape with a very thin copper-plated layer. Then we wound the pancake with 40-N winding tension. After finishing the bottom pancake winding, we inserted an annulus Kapton film on the surface of the bottom pancake coil and wound the top pancake coil as shown in Figure 2(c). The top pancake winding process similar with the bottom pancake coil winding process described above.

3.2. DP test and extra shunting

We made a total of six DP coils and named each DP as DP A to DP F; DPs A, B, C, and D are composed of two 6-mm single pancake coils, and DPs E and F are composed of 6-mm and 8-mm single pancake coils. Each DP coil was tested in a liquid nitrogen bath. We estimated the critical current by following equation [16]:

$$I_c(\theta, B) = I_{c0}\left[1 + \epsilon\left(\frac{B}{B_0}\right)^{\alpha}\right]^{-\beta}, \quad (1)$$

where I_c is the critical current, θ is the magnetic field angle, B is the magnitude of the field, I_c0 is the self-field critical current at 77 K, α, β, are constant values for the REBCO tape. The ϵ is defined as

$$\epsilon = \sqrt{sin^2(\theta) + cos^2(\theta)/\gamma^2}, \quad (2)$$

where γ is also a constant value of the REBCO tape. The value of I_{c0} is 280 A, B_0 is 0.08083, α is 1.00,

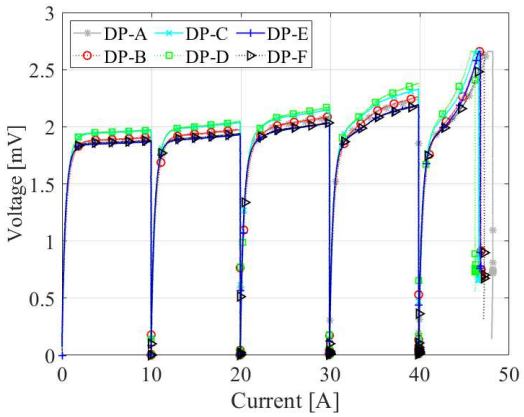

Figure 3. Critical current testing result of each DP coil at liquid nitrogen before shunting.

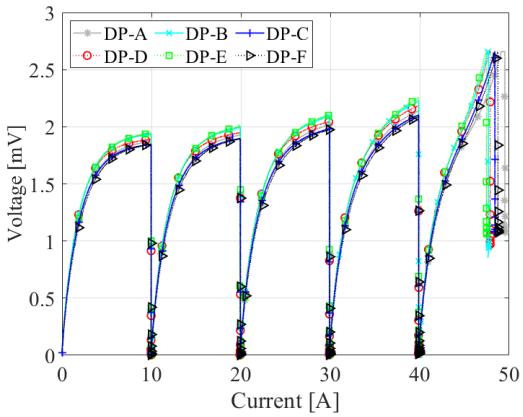

Figure 5. Critical current testing result of each DP coil at liquid nitrogen after shunting.

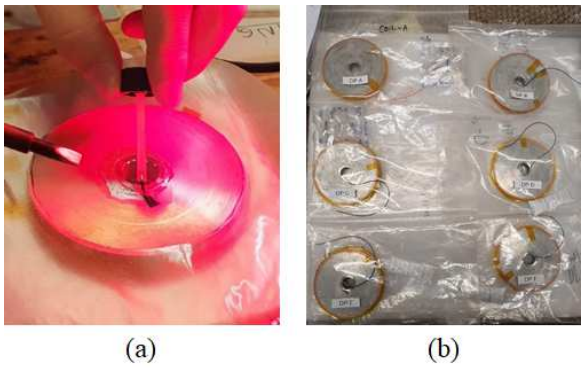

Figure 4. Extra shunting by soldering. (a) is the surface soldering process, (b) is the soldered pancakes after testing. The coils stored inside a plastic bag with moisture absorber.

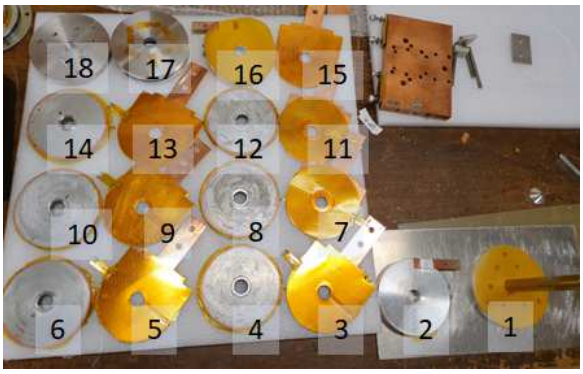

Figure 6. Assembly parts for the magnet. The numbered parts are for the coil assembly. The upper right side rectangular copper block without a part number is a coldhead connection adaptor.

β is 0.72, and γ is 4.35[16]. The estimated minimum critical current of the DP coils is 48.5 A. We measured the voltage vs. current (I-V) characteristic of the DP coils in liquid nitrogen. Figure 3 shows the result. Every DP showed similar behavior, including DP E and DP F, containing C1 and C12. We stopped the current when the voltage rose and measured steady-state voltage above 250 μV from 46.1 A to 48.0 A. The average resistance of individually measured six inner joints was 176.3 nΩ with a standard deviation of 1.8 nΩ and the average characteristic resistance, R_c, representing an average radial-direction resistance of the NI DP coil, was 4.3 mΩ with a standard deviation of 0.3 mΩ.

After finishing the initial liquid nitrogen test, we have applied $In_{52}Sn_{48}$ solder on the top and bottom surfaces of each DP coil as an extra shunting for the extreme NI coil. This extra shunting reduces the contact resistance between turns and provides additional current paths if any defective part appears inside the coil[17, 18]. Figure 4(a) shows the extra shunting process. The tip temperature of the soldering iron was set around 190 ℃, and the heating plate, where the DP coil was put on during soldering, was warmed up to 70 ℃. An infrared heater was also used to heat the ambient temperature around the surface. Figure 4(b) is a photo of the extra shunt applied DP coils. As shown in Figure 5, there was no significant change in critical current. As expected, shunting decreased the average R_c value from 0.4 mΩ to 0.1 mΩ.

3.3. Outer joint and coil assembly

Figure 6 is the photo of the magnet parts. The part number 1 is a center tubing with insulation Kapton tape on it. The parts number 2 and 16 are current leads, the parts number 3, 5, 7, 9, 11, 13, 15 are cooling plates, parts number 4, 6, 8, 10, 12, 14 are DP coils, and parts number 17 and 18 are the pre-loading plate and the bottom plate. We sequentially assembled the coil from the part number 1 to 18. The assembly process starts from the top plate and the center tubing, part number 1. The positive current terminal, part number 2 is stacked upon the Kapton

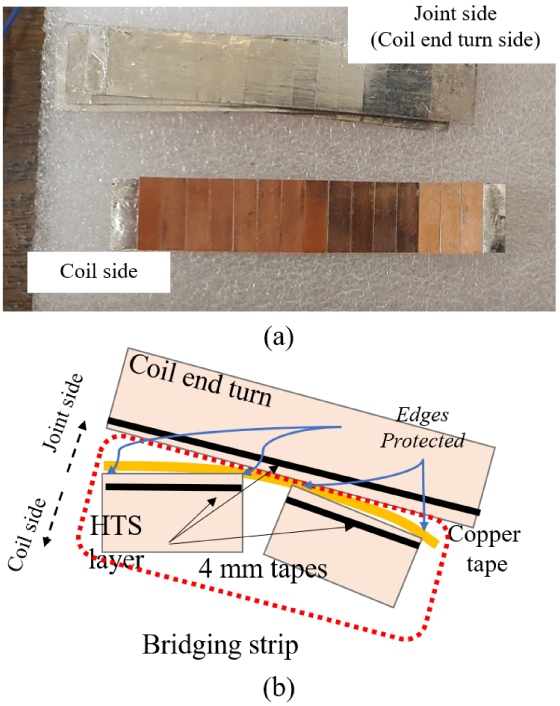

Figure 7. The bridging strip is used for the outer joint. (a) is the photo of the bridging strip used to connect DP to DP joint. (b) is the concept of edge protection by the bridging strip.

insulation attached on the top plate. Next part number 3 is the cooling plate. We have prepared copper cooling plates with Kapton insulation. An insulated heater for controlling temperature attached to the each cooling plate. We also added Kapton tapes on both sides of the plate for insulation. The rest parts were sequentially assembled from parts number 4 to 18. After the coil stack assembly had finished, about 1,000 kg pre-loading was applied with the bolts to secure the mechanical stability of the entire structure.

We used bridging strips to make the outer joints. Figure 7(a) shows the bridging strips for the outer joint. A bridging strip has a total of fifteen 4 mm HTS tapes soldered onto the 0.0254 mm copper sheet, which has 12 mm width according to its joint location. The HTS side is faced with the copper sheet, and the joint is connected through this copper sheet. Figure 7(b) shows the concept of the edge protection. The copper sheet covers the edges of the 4 mm HTS tapes and prevents stress concentration from the edges when we press the joint part. Figure 8(a) shows the pre-tinning process of the coil. We applied solder to the both sides of the coil end turn. The HTS side is for joint, and the other side is for higher heat conductivity while soldering process using liquefied solder. Figure 8(b) is the process of inserting the bridging strip to the soldering position. Figure 8(c) shows applying load

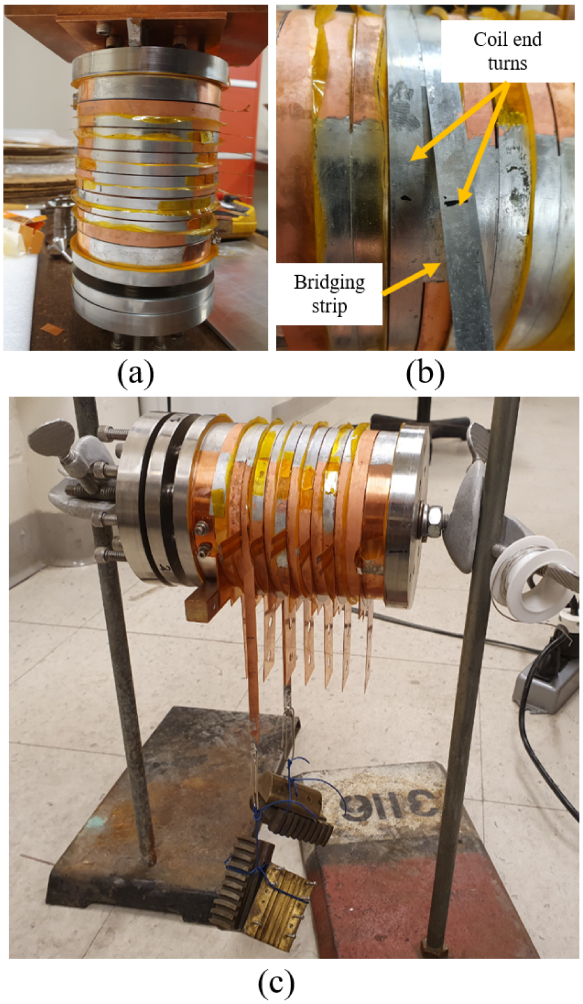

Figure 8. Outer joint process for the magnet. (a) shows the pre-tinned . (b) is the photo of applying force to press outer joint.

during the outer joint process. We have applied a load of about 200 g to uniformly press the conductors and the bridging strip during outer joints. We used a flat type soldering iron to heat the joint. The temperature was set around 220 ℃. After finishing the outer joints, the outside of the coil is covered with 6 mm stainless steel tape or 8 mm Hastelloy tape to prevent any scratch or contamination from the outside environment.

3.4. Instrumentation and cryostat assembly

Figure. 9(a) shows the instrumentation schematics. There are two Hall sensors, one at the center of the coil and the other is at the top of the coil. We have used a total of five Cernox sensors, located at the topmost cooling plate, bottom-most cooling plate, positive terminal, negative terminal, and the second stage. We also used three platinum sensors

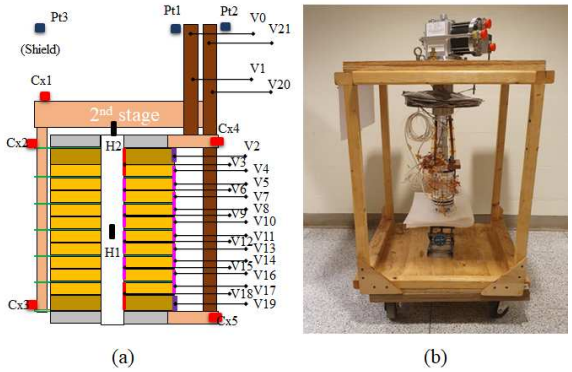

Figure 9. Assembled magnet. (a) is sensor and voltage tap schematics and (b) is the completed magnet.

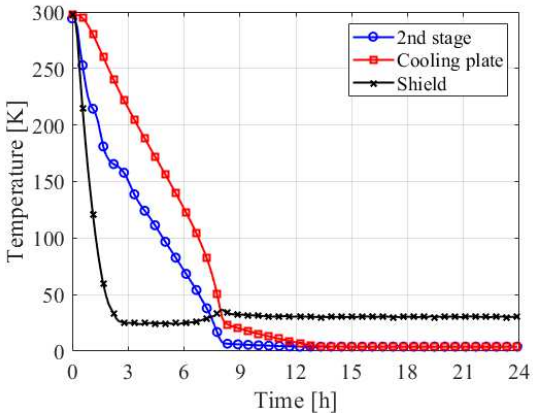

Figure 10. The initial cooling of the magnet. The 1st stage for the shield cooled around 30 K and the 2nd stage for the magnet cooled below 4 K.

for the current leads and radiation shield temperature measurement. Each DP has three voltage taps. One is from the winding bobbin, which is a center tap of the DP, and the other two taps from the location right before starting point of the outer joints. The control heater was operated in a parallel connection. Figure 9(b) is the assembled magnet. We have used a Sumitomo RDK408D for the cryocooler. The 5-gauss line are 1.2 m in radial direction, and 1.4 m in axial direction from the center of the magnet when it is fully charged.

4. Magnet operation

4.1. Initial cooling

The initial cooling result is shown in Figure 10. The cooling plate, which represents the magnet temperature, cooled below 4.0 K after 14 hours and remained stable after around 20 hours. The radiation shield temperature stabilized at about 30 K. We have calibrated the temperature-control-heater attached on

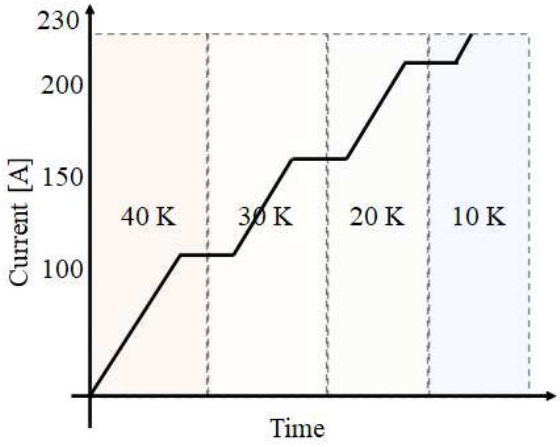

Figure 11. The concept of Temperature-Controlled Charging Sequence (TCCS) for magnet operation.

the cooling plates after the initial cooling. The magnet temperature stabilized 10 K, 20 K, 30 K, and 40 K at the heater wattage 1 W, 5.2 W, 10.5 W, and 15 W, respectively. We used the wattage values as an initial reference for the temperature control and adjusted the wattage during the experiment based on the temperature monitoring results.

4.2. SCS reduction by low margin ramping sequence

We need to reduce the peak screening-current-induced stress (SCS) before it reaches a critical level. There are several ways to suppress the screening-current. For example, the current sweep reversal (CSR) method is one of the most effective ways to reduce the remaining screening current-induced field[19]. However, CSR is not applicable to suppress the peak SCS because it requires pushing the screening current to the peak level at least one time. Therefore, we have introduced a new Temperature-Controlled Charging Sequence (TCCS) method. TCCS method works by changing the magnet temperature, gradually while charging up the magnet. At the initial point of charging, the critical current of the magnet is decreased due to the high initial temperature[20, 21]. This reduced critical current also reduces the screening current during the charging sequence. Figure. 11 shows the initial plan of the TCCS method for the magnet. A slow normal zone propagation under enough cooling capacity is essential for using the TCCS. In this case, the magnet has extreme no-insulation with solder shunting, making very slow NZPV and enough cooling capacity using cooling plates between DPs. Figure 12 shows measured center field at 100 A with different temperatures. Because of the screening field, the field is smaller than the ideal case. However, the difference is much smaller at 40 K compared to the 10 K.

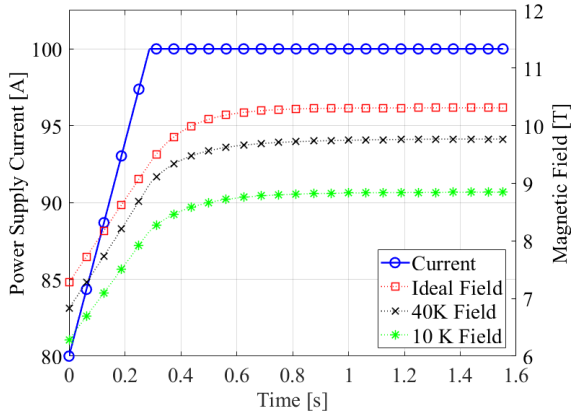

Figure 12. The center magnetic field at 100 A. The ideal field result is only considering the NI effect. The field is lower due to the screening current, and it became lower at the lower temperature.

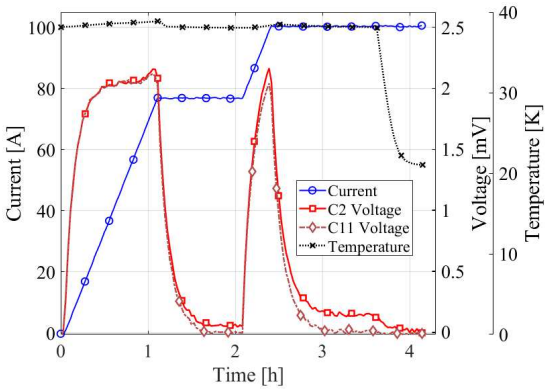

Figure 13. The resistive voltage at C2. The voltage decreased as we lower the temperature.

4.3. Hot-spot and voltage spike analysis

The initial charging started at 40 K, 0 A to 100 A, 0.02 A/s. Figure 13 shows the current, C2, C11, and magnet temperature data from initial ramping. As a resistive voltage was detected inside C2 during ramping around at 80 A, we stopped the ramping, waited around 1 hour, and charged it again up to 100 A. The resistive voltage acted like a damaged HTS section, with a very low critical current value. This resistive characteristic was not seen at the individual DP coil testing after extra shunting. The C2 might be damaged during the assembly or outer jointing process. We can estimate the length of the damaged section from the measured resistance value 1.5 $\mu\Omega$ at 40 K, 100 A. It corresponds to a normal resistance of 0.11-mm long REBCO tape calculated by using the copper and silver matrix of 6 mm wide, 3.5 µm thick and the equivalent resistivity of 0.28 nΩ·m at 40 K. Based on this calculation, the damage seems

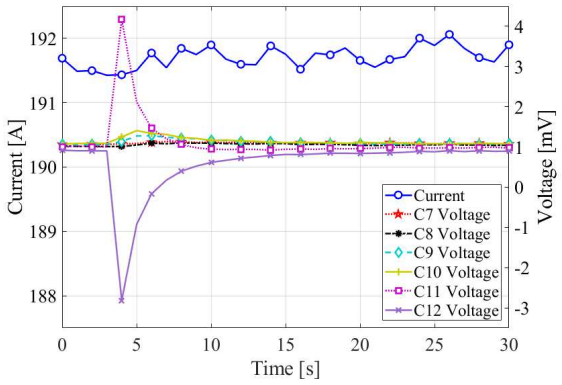

Figure 14. The voltage spike during magnet charging process. The peak voltage appeared in C12 and the magnitude decreases as the distance become farther from the C12.

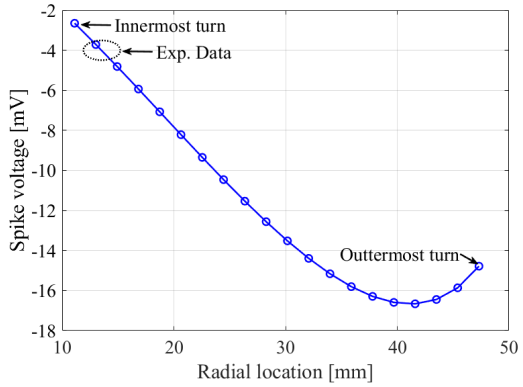

Figure 15. The expected peak spike voltage according to the defective spot location.

to be caused by sharp-edged material pressing the HTS side. However, the actual length may be much longer than this if we consider the NI effect of the magnet. Since the heat generated from the hot spot is lower than 80 mW even at 228 A, which is lower than the single heater power at 10 K (200 mW), we continued charging the magnet. However, we have turned off the heater at this initial attempt considering the heat concentration at the defective region. While ramping up, we have encountered a voltage spike around 191.5 A. Figure 14 shows the voltage spike data. The highest voltage spike appeared in C12 in a negative direction, and it propagated upward throughout the entire coil. When a resistive component appears in a NI coil, the defective turn rapidly loses the current, which looks like a disappearing turn. If the operation current remains constant during this transient situation, we can estimate the location of this defective component using this disappearing turn behavior,

$$V_{spike} = \frac{d(LI)}{dt} = L\frac{dI}{dt} + I\frac{dL}{dt} \approx \frac{I(L_{N-1} - L_N)}{\Delta t} \qquad (3)$$

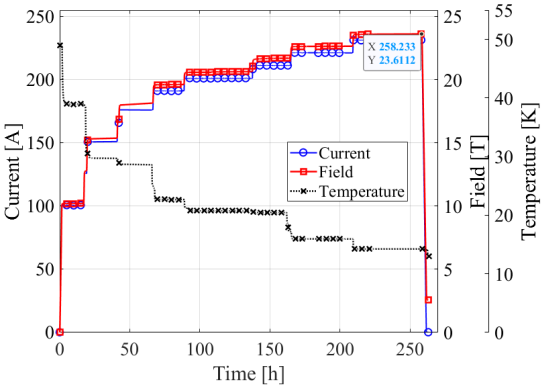

Figure 16. The current, field and temperature of the magnet up to 23.6 T.

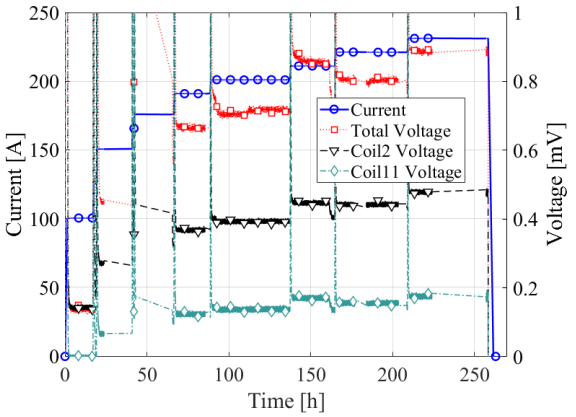

Figure 17. C2, C11, and the total voltage during the charging. Almost half of the voltage is generated from C2.

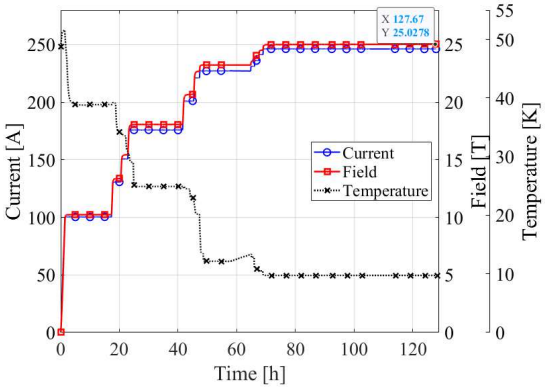

Figure 18. The current, field, and temperature profile of the coil during ramping up to 25 T.

where V_{spike} is the spike voltage, L is time-dependent inductance of the coil, I is the operating current, L_{N-1} is the inductance of coil without the defective turn, L_N is the inductance of entire turn coil, and Δt is the time interval between data points. The Δt in this data set is 1 s. Since L_{N-1} is a function of the location of defective turn, we can calculate the spike voltage as a function of the location of defective turn in the C12. Figure 15 shows the result of the calculation. Based on this calculation, the defective turn seems to be located inner section of the coil, which has the highest stress concentration due to the screening current. Even though the exact source of this spike is not sure, the relationship between this spike and the screening current induced stress is one of the most expected candidates. After detecting two more voltage spikes while ramping near 198 A, a similar level, we stopped ramping the magnet.

4.4. 23.5 T and 25 T operation

We started charging the magnet again with the TCCS method after warming up the magnet over 100 K to clean the remaining screening current. Figure 16 shows the ramping up and down result using TCCS. The initial starting temperature was set to 50 K, and the temperature profile followed the original plan shown in figure 11, however, modified a little monitoring the voltage, especially C2. Figure 17 shows the total magnet voltage, C2 voltage, and C11 voltage during the TCCS ramping up. Almost half of the magnet voltage was occupied by the resistive component of the C2. The 23.6 T center field obtained 230 A at 14.2 K with 1.9 W heater operation. Total magnet voltage was 0.89 mV at 230 A, about 200 mW heat generated on the magnet side. We ramped down the magnet at 14.2 K, and the remnant field was about 2.5 T. We had warmed up the magnet and charged it up again up to 25 T. Figure 18 shows the current, field, and temperature profile of the TCCS. The base TCCS profile is the same as the previous sequence, but it was adjusted slightly by monitoring the coil voltage and temperature signals. The center field is set to 25 T at 245 A, at 10 K. The field was sustained about for 60 hours.

5. Next Steps Toward a Benchtop 1-GHZ NMR

As we successfully demonstrated the feasibility of a compact, cryogen-free, high-field REBCO magnet, we will move forward to the next step towards a benchtop 1-GHz NMR. We will refine the magnet design from our previous first-cut design [9] and build a cryogen-free, shielded all-REBCO 23.5-T/25-mm-RT-bore magnet, and then convert this non-NMR-field 23.5-T magnet to a NMR-grade magnet having a high homogeneity. The key design requirements are summarized in Table 2. This benchtop magnet will incorporate all the innovative design, manufacturing and operation

Table 2. Target requirements of the benchtop NMR

Parameter	Target Value
Center field	23.5 [T]
Cooling method	Cryogen-free
RT bore	25 [mm]
Field homogeneity	<0.1 [ppm] (@5-mm-diameter, 10-mm-length cylindrical volume)
5-gauss line	(Radial) ≤1.5 [m] (Axial) ≤2 [m]

concepts validated by the prototype magnet. We intend to adopt a passive shielding by using iron to reduce the 5-gauss radius within 1.5 m, which is less than half of the commercial ultra-shielded 1-GHz magnets. The screening current is still a challenging problem for both field homogeneity and field stability. We first reduce the screening current considerably with our proposed TCCS, and then, to achieve a target field homogeneity, we will adopt superconducting/copper shim coils and ferromagnetic shimming. We envision this benchtop cryogen-free 1-GHz microcoil NMR magnet will become a very powerful and affordable research tool for the NMR based structural biology community who eagerly anticipates higher operating frequencies.

6. Conclusion

We designed, constructed, and operated an all-REBCO conduction-cooled 23.5-T magnet. We applied the extreme NI winding technique that incorporates solder shunting in each pancake. The extreme NI magnet and the system cooling suppressed heat generation at a resistive defect section in one of the pancakes. We used a temperature-controlled charging sequence TCCS to reduce the peak screening-current-induced stress (SCS). When the TCCS was not appropriately applied, multiple voltage spikes occurred, for which we believe that SCS is the most likely source. Applying TCCS, we successfully charge the magnet up to 23.6 T at 14 K without voltage spikes. We further tested up to 25 T at 10 K, and kept it at 25 T for nearly 60 hours.

Acknowledgement

This work was supported by the National Institute of General Medical Sciences of the National Institutes of Health under Award R21GM129688.

References

[1] Lin W C and Fedder G K 2001 *A Comparison of Induction-Detection NMR and Force-Detection NMR on Micro-NMR Device Design* (The Robotics Institute School of Computer Science Carnegie Mellon University)

[2] Jonathan V Sweedler, Richard L Magin, Timothy L Peck and Andrew G Webb 2000 Microcoil based micro-NMR spectrometer and method

[3] Magin R, Webb A and Peck T 1997 *IEEE Spectrum* **34** 51–61 ISSN 0018-9235

[4] Hashi K, Ohki S, Matsumoto S, Nishijima G, Goto A, Deguchi K, Yamada K, Noguchi T, Sakai S, Takahashi M, Yanagisawa Y, Iguchi S, Yamazaki T, Maeda H, Tanaka R, Nemoto T, Suematsu H, Miki T, Saito K and Shimizu T 2015 *Journal of Magnetic Resonance* **256** 30–33 ISSN 10960856

[5] Hahn S, Kim K, Kim K, Hu X, Painter T, Dixon I, Kim S, Bhattarai K R, Noguchi S, Jaroszynski J and Larbalestier D C 2019 *Nature* **570** 496–499 ISSN 14764687 URL http://dx.doi.org/10.1038/s41586-019-1293-1

[6] Bai H, Abraimov D V, Boebinger G S, Bird M D, Cooley L D, Dixon I R, Kim K L, Larbalestier D C, Marshall W S, Trociewitz U P and Weijers H W 2020 *IEEE Transactions on Applied Superconductivity* **30** ISSN 15582515

[7] Liu J, Wang Q, Qin L, Zhou B, Wang K, Wang Y, Wang L, Zhang Z, Dai Y, Liu H *et al.* 2020 *Superconductor Science and Technology* **33** 03LT01

[8] Wikus P, Frantz W, Kümmerle R and Vonlanthen P 2022 *Superconductor Science and Technology* **35** 033001 ISSN 0953-2048

[9] Park D, Choi Y H and Iwasa Y 2019 *IEEE Transactions on Applied Superconductivity* **29** ISSN 15582515

[10] Hahn S, Park D, Bascuñán J and Iwasa Y 2010 *IEEE Trans. Appl. Supercond.* **21** 1592–1595

[11] Lee W, Park D, Choi Y, Li Y, Bascuñán J and Iwasa Y 2021 *IEEE Transactions on Applied Superconductivity* **31** ISSN 15582515

[12] Park D, Lee W, Li Y, Choi Y, Bascuñán J and Iwasa Y 2019 Test Results and Analysis of a Single Pancake Validation Coil for a Cryogen-Free 23.5 T/ϕ15 mm REBCO Magnet

[13] Park D, Lee W, Bascuñán J and Iwasa Y 2020 A Conduction-Cooled 23.5-T REBCO Magnet Prototype Towards a Tabletop 1-GHz Microcoil NMR Magnet: Extreme No-Insulation Coil Test Results

[14] Park D, Lee W, Bascuñán J, Kim H M and Iwasa Y 2021 Operation Results of a 23.5-T REBCO Magnet Prototype Towards a Tabletop Liquid-Helium-Free 1-GHz Microcoil NMR

[15] Park D, Lee W, Bascuñán J, Kim H M and Iwasa Y 2022 *IEEE Transactions on Applied Superconductivity* **32** 1–5

[16] Zhang X, Zhong Z, Geng J, Shen B, Ma J, Li C, Zhang H, Dong Q and Coombs T A 2018 *Journal of Superconductivity and Novel Magnetism* **31** 3847–3854 ISSN 15571947

[17] Lee W S, Lee J, Song S, Park Y G, Jin H, Hahn S, Ahn M C and Ko T K 2015 *IEEE Transactions on Applied Superconductivity* **25** ISSN 10518223

[18] Mun J, Lee C, Sim K, Lee C, Park M and Kim S 2020 *IEEE Transactions on Applied Superconductivity* **30** ISSN 15582515

[19] Yanagisawa Y, Kominato Y, Nakagome H, Fukuda T, Takematsu T, Takao T, Takahashi M and Maeda H 2012 Effect of coil current sweep cycle and temperature change cycle on the screening current-induced magnetic field for ybco-coated conductor coils *AIP Conference Proceedings* 57 pp 1373–1380 ISBN 9780735410206 ISSN 0094243X

[20] Kajikawa K and Funaki K 2011 *Superconductor Science and Technology* **24** ISSN 09532048

[21] Wang L, Wang Q, Qin L, Wang K, Liu J and Hu X 2020 *Journal of Superconductivity and Novel Magnetism* **33** 1729–1735 ISSN 15571947